Flexoelectric thin-film photodetectors

Ming Wu[1,3,#], Zhizheng Jiang[2,#], Xiaojie Lou[1,*], Fan Zhang[4], Dongsheng Song[5], Shoucong Ning[3], Mengyao Guo[1], Stephen J. Pennycook[3,*], Ji-yan Dai[4], Zheng Wen[2,*]

[1]Frontier Institute of Science and Technology, State Key Laboratory of Electrical Insulation and Power Equipment, and State Key Laboratory for Mechanical Behavior of Materials, Xi'an Jiaotong University, Xi'an 710049, P. R. China

[2]College of Physics and Center for Marine Observation and Communications, Qingdao University, Qingdao 266071, P. R. China

[3]Department of Materials Science and Engineering, National University of Singapore, 9 Engineering Drive 1, 117575, Singapore

[4]Department of Applied Physics, The Hong Kong Polytechnic University, Hung Hom, 999077 Kowloon, Hong Kong

[5]Ernst Ruska-Centre for Microscopy and Spectroscopy with Electrons, Forschungszentrum Jülich, D-52425 Jülich, Germany,

[#] Ming Wu and Zhizheng Jiang contributed equally in this work.

[*]Corresponding author Email addresses:

xlou03@mail.xjtu.edu.cn (Xiaojie Lou)

steve.pennycook@nus.edu.sg (Stephen J. Pennycook)

zwen@qdu.edu.cn (Zheng Wen)

Keywords

Flexoelectric effect, photovoltaic effect, heterostructure, thin film, strain gradient

Abstract

The flexoelectric effect, which manifests itself as a strain-gradient-induced electrical polarization, has triggered giant interest due to its ubiquitous existence in crystalline materials without the limitation of lattice symmetry. Here, we propose a flexoelectric photodetector based on a thin-film heterostructure. This prototypical device is demonstrated by epitaxial $LaFeO_3$ thin films grown on $LaAlO_3$ substrates. A giant strain gradient of the order of 10^6 /m is achieved in $LaFeO_3$ thin films, giving rise to an obvious flexoelectric polarization and generating a significant photovoltaic effect in the $LaFeO_3$-based heterostructures, with nanosecond response under light illumination. This work not only demonstrates a novel self-powered photodetector different from the traditional interface-type structures, such as the p-n and Schottky junctions, but also opens an avenue to design practical flexoelectric devices for nanoelectronics applications.

It is well known that strain engineering can change lattice structure and modulate electronic, magnetic, and optoelectronic properties of crystalline materials. A number of intriguing functionalities absent in their bulk counterparts are therefore created in strained thin-film heterostructures. For example, uniform in-plane strains induce room-temperature ferroelectricity in paraelectric $SrTiO_3$ (STO) heterostructures [1] and nanometer-scale polar-skyrmion bubbles in $(PbTiO_3)_n/(STO)_m$ superlattices [2]. Furthermore, with a strain gradient that breaks inversion symmetry, an electric polarization, *i.e.*, a flexoelectric polarization (P_l), can be generated in centrosymmetric materials due to the flexoelectric effect, which provides new opportunities for the manipulation of their physical properties. The P_l is given by [3]

$$P_l = \mu_{ijkl} \frac{\partial e_{ij}}{\partial x_k} \tag{1}$$

where $\partial e_{ij}/\partial x_k$ is the strain gradient and μ_{ijkl} the flexoelectric coefficient, which scales with the dielectric susceptibility of the material (ε_{ij}) and obeys $\mu_{ijkl} = \gamma_{kl}\varepsilon_{ij}\frac{e}{a}$ (γ_{kl} is a constant related to the material, e the electron charge, and a the lattice constant). As a fourth-rank tensor determined physical phenomenon, the flexoelectric effect can exist in all 32 point groups regardless of the lattice symmetry [3]. This ubiquitous feature provides a wide material selection for the design of flexoelectric devices with diverse functionalities. Typical examples are complex oxides, in which the asymmetric loading of stresses applied on trapezoid-shape structures (Figure 1a) and flexure-mode composites first demonstrated flexoelectric effects in nonpiezoelectric materials, revealing the possibilities of giant piezoelectric responses comparable with or beyond those achievable in ferroelectrics [4-7].

Given that the strain gradient is inversely proportional to the material dimension, the flexoelectric effect may become more pronounced and affect physical properties more

significantly with decreasing feature size. For example, bendable devices (Figure 1b) with specially designed structures of $Pb(Zr,Ti)O_3$ ribbons, $(Ba,Sr)TiO_3$ beams, and $SrTiO_3$ micro-cantilevers can generate a strain gradient of $10^{-1} \sim 10^4$ /m. These structures have been utilized in energy harvesters [8-9], curvature sensors [8], and actuators[10]. Shu et al reported that flexoelectric effect in halide perovskites can be enhanced by orders of magnitude by illumination and therefore beneficial for its application in energy harvesting[11]. By using scanning transmission electron microscopy (STEM), Tang et al[12] observed strain gradients at the centers of flux closure domains in ferroelectric films as high as 10^9 /m. Enhanced nanoscale flexoelectric effects have also been achieved by using the atomic force microscopy (AFM) technique, in which the AFM tips apply loading forces and induce strain gradients underneath the sample surface. Therefore, mechanical modulations of various electrical properties, such as the ferroelectric polarization switching [13-14], the migration of charged defects [15], the mechanical control of charge-carrier transport[16-17], and the strain gradient-induced photovoltaic effect [18], have been observed. Lee et al demonstrated a flexoelectricity-controlled rectification effect in epitaxial $HoMnO_3$ thin film[19]. In addition, it has been observed that the flexoelectric polarization can modulate electron transport of 2-dimensional electron gases in $LaAlO_3$/STO heterostructures[20]. These advances suggest giant potential for the application of the flexoelectric effect in nanoelectronics devices.

Here, we propose a flexoelectric photodetector based on thin-film heterostructures. As depicted in Figure 1c, this optoelectronic device has a two-terminal metal/oxide/metal structure, in which a strain gradient along the out-of-plane direction is introduced in the oxide layer by gradually relaxing the heteroepitaxial lattice-mismatch strain between the film and substrate. The inherently-formed nonlocal strain gradient generates a flexoelectric polarization throughout the oxide layer (Figure 1c). Under light illumination, the photo-excited carriers are separated and migrate toward the metal electrodes due to the flexoelectric polarization induced band bending in the oxide layer (Figure 1d). As a result, we observed a photovoltaic effect with photocurrent of 0.3 mA/cm^2 and a photovoltage of 0.4 V,

which is comparable to junction-based photodetectors. In addition, owing to the universal existence of the flexoelectric effect, the proposed photodetector can be customized by diverse materials [18, 21-24] with band gaps matching the wavelength of light to be detected, as shown in Figure 1e.

In the present work, a perovskite oxide $LaFeO_3$ (LFO), which exhibits a bandgap of ~2.6 eV (Figure S3), corresponding to a wavelength of 475 nm (blue light), is selected as the photoactive layer. LFO has an orthorhombic perovskite structure, with an average pseudocubic lattice parameter of 3.924 Å, facilitating epitaxial growth on commercial single crystalline substrates. Pseudocubic (001)-oriented LAO is adopted as the substrate, which has a lattice constant of a=3.81 Å, resulting in a large compressive strain of 2.99% in the LFO layer. Ultrathin $LaNiO_3$ (LNO) with a thickness of 6 nm is first grown on the LAO substrate as the bottom electrode. As a comparison, we also grow LFO thin films on cubic (001)-oriented STO substrates (a=3.905 Å). The lattice mismatch between LFO and STO is only 0.48%, much smaller than that on the LAO substrate. Figure S1a shows X-ray diffraction patterns of LFO/LNO/LAO and LFO/LNO/STO heterostructures, in which only (00*l*) Bragg reflections can be observed in a 2θ range of 42° to 50°, suggesting epitaxial growth of the LFO thin films. In addition, due to the larger in-plane compressive strain, the (002) Bragg reflection of LFO/LNO/LAO locates at a lower 2θ than that of the LFO/LNO/STO. AFM images (Figure S1b) indicate atomically-smooth surfaces of the LFO thin films with a root-mean-square roughness of ～0.1 nm.

As shown in Figure 2, the lattice structure of the LFO thin films is visualized by means of STEM using atomic resolution high angle annular dark field (HAADF) images. Because the

brightness of the HAADF image is approximately proportional to Z^2 (Z is the atomic number), the brightness of heavier atoms is much higher than that of lighter atoms [12]. As shown in Figure 2c and 2e, the LFO thin films show cube on cube growth on both the LAO and STO substrates and the interfaces between the LFO layers, the LNO bottom electrodes, and the substrates (LAO or STO) can be easily distinguished, as indicated by the cyan dashed lines. The thickness of the LFO thin films is therefore determined as 11.5 and 10.5 nm on LAO and STO, respectively. The relaxation of heteroepitaxial misfit strain is quantified by geometric phase analysis (GPA) [12, 25-26], and the distributions of in-plane strain e_{xx} calculated relative to the substrate are demonstrated in Figure 2d and 2f, respectively, for the LFO/LNO/LAO and LFO/LNO/STO heterostructures. One can find that the strains in the 6 nm-thick LNO bottom electrodes are almost the same as that of the LAO and STO substrates, indicative of the coherent epitaxial growth of the ultrathin LNO, which facilitates the strain modulation of the upper LFO layers with the substrates. For the LFO on LAO substrate, a terraced color mapping with increasing e_{xx} from ~0 at the LFO/LNO interface (light yellow) to ~0.04 at the surface (dark green) is observed, as shown in Figure 2d. The gradual relaxation of in-plane strain is realized by the formation of dislocations, as indicated by the dashed red circle in Figure 2c. A line profile of the e_{xx} in the representative region along the blue arrow in Figure 2d is plotted in Figure 2g for clarity. The in-plane strain increases linearly from ~0 up to 3.8 % in the LFO layer within a thickness of 11.5 nm, which results in a strain gradient $\partial e_{xx}/\partial z_k$ of ~3×10^6 /m along the [001] direction (Figure 2g). However, in the LFO/LNO/STO heterostructure the calculated e_{xx} is *ca*. 0.3% (Figure 2h), smaller than 0.5 %, the resolution limitation of the GPA method [27-28], and no obvious strain gradient can be observed. (More

details about the structure relaxation of the LFO thin films on STO substrates with different thickness are shown in Figure S14.) 2-dimensional distribution of the strain gradient of the LFO thin films with different thickness can be seen in Figure S8.

The effective flexoelectric coefficient μ_{xz} of 70 nC/m of the LFO thin films is measured using a cantilever beam bending method (Figure S4). However, it should be noticed that such value includes contribution from both flexoelectric response and piezoelectricity, which cannot be distinguished from each other[29-30]. The electron energy loss spectra of the L edge of Fe were also recorded by STEM (Figure 2i, Figure S5). The L edge is induced by electron transitions from the 2p to 3d orbitals, and hence, the oxidation state of Fe ions can be revealed [31]. It is observed that the L_3 peak of the LFO thin film on the LAO substrate (Line profile 1, 2) shifts to a lower energy compared with that of the LFO on STO (Line profile 3, 4), which indicates a lower oxidation state of Fe in the LFO/LNO/LAO heterostructure. The reduction of Fe ions may be a result of the trapping of electrons in the LFO layer, which screen the flexoelectric polarization, or could indicate the presence of oxygen vacancies, which are known to be one method for strain relaxation[32-34].

The effect of flexoelectric polarization on the band structure of Pt/LFO/LNO is depicted in Figure 3a and 3b. Figure 3a depicts the band diagram of a Pt/LFO/LNO heterostructure without considering the existence of flexoelectric polarization. It can be seen that the Schottky barriers $\emptyset'_{B01}$ and $\emptyset'_{B02}$ at Pt/LFO and LFO/LNO interfaces are 1.6 eV and 0.8 eV, respectively, compared to the work function of Pt (5.3 eV), LNO (4.5 eV), and the electron affinity of LFO (3.7 eV). The Schottky junction contributed photovoltaic effect is therefore dominated by the higher Schottky barrier at Pt/LFO interface. The photogenerated carriers

can be separated and the electrons (holes) would flow out (into) Pt electrodes. In such case, the photovoltaic current density-voltage (*J-V*) curve would appear in the fourth quadrant as shown in Figure 3c. (Voltage is applied on the top metal electrode while the LNO bottom electrode is grounded). However, when taking flexoelectric polarization into consideration, the band diagram of the Pt/LFO/LNO heterostructure is expected to be tuned, as the appearance of polarization is always companied by band tilting[35-36]. The actual barrier heights at the Pt/LFO (Φ_{B01}) and LFO/LNO (Φ_{B02}) interfaces in the Pt/LFO/LNO/LAO device are 1.22 eV and 1.25 eV, respectively, as revealed by fitting the dark *J-V* curve with a thermal emission mechanism (Figure S6 and supporting text 7), and the band diagram is depicted in Figure 3b. It is observed that the energy band tilting direction is opposite to the case in Figure 3a. Under illumination, the separated electrons (holes) would flow into (out) Pt, and therefore the photovoltaic current density-voltage (*J-V*) curve would appear in the second quadrant as shown in Figure 3c.

The photovoltaic effects of Pt/LFO/LNO devices are shown in Figure 4a. For the 11 nm-thick LFO on LAO substrate under blue light illumination, a significant photovoltaic effect with a short-circuit current density (J_{sc}) of 0.21 mA/cm^2 and an open circuit voltage (V_{oc}) of -0.2 V is observed in the second quadrant, indicating that the flexoelectric effect dominates the photocurrent, according to Figure 3c. In addition, with decreasing work function of the top electrode, the flexoelectric-induced band tilt should become more pronounced and, as a result, the absolute value of V_{oc} observed in the metal/LFO/LNO/LAO devices increases (Figure S7). These results confirm the dominant effect of the flexoelectric polarization in determining the photovoltaic effect in Pt/LFO/LNO devices.

However, the I-V curve of the 11 nm Pt/LFO/LNO/STO device under illumination does not appear in the fourth quadrant. Instead, it crosses the zero point, which indicates no photovoltaic effect exists in the sample. The I-V curves and the relaxation of the LFO thin films of different thicknesses on STO substrates were further studied (see the supporting text 11 in the Supporting information attached). These results suggest that the relaxation of misfit strain also occurs in the 11 nm LFO/LNO/STO structure, but the induced flexoelectric polarization is very weak and its effect is canceled out by the Schottky contacts (see the discussion in the supporting text 11).

Since both the strain relaxation and the strain gradient $\partial e_{xx}/\partial z_k$ are closely related to the film thickness (Figure S8 and Figure S9), the dark and illumination current density-voltage (*J-V*) curves of Pt/LFO/LNO/LAO devices are measured as a function of LFO thickness (Figure S10). The values of V_{oc} and J_{sc} extracted are plotted in the inset in Figure 4a for clarity. As shown, the photovoltaic effect appears in Pt/LFO/LNO/LAO devices with thickness above 11 nm. In addition, the V_{oc} increases with increasing LFO thickness from 11 to 50 nm, while the J_{sc} peaks at an optimized thickness of 35 nm. The decrease of J_{sc} in the 50 nm-thick LFO may be a result of the scattering of carriers by twist/tilt boundaries that are formed to release the rapidly increasing elastic energy with increasing thickness. More details about the structural relaxation of LFO heterostructures with varying thickness are characterized and discussed in the supplementary information (Supporting text 9).

Figure 4b shows power density dependent *J-V* curves of a 35 nm-thick Pt/LFO/LNO/LAO device. One can see that J_{sc} increases linearly with increasing power density up to 20 W/cm^2, while the V_{oc} stays almost unchanged. The time-dependent J_{sc} without an applied bias is shown in Figure 4c, in which the Pt/LFO/LNO/LAO photodetector exhibits stable response to repeated light on/off cycles. In addition, when excited by a nanosecond laser pulse (Figure

S2), the device shows an ultrafast response of about 15 ns full width half maximum (FWHM, the inset in Figure 4c). The nanosecond photoresponse of the flexoelectric photodetector may benefit from the ultrafast carrier dynamics in perovskite oxides [37]. Moreover, the responsivity and detectivity, which demonstrate the sensitivity of a photodetector to light [38], are evaluated over a wide temperature range, as shown in Figure 4d and discussed in supporting text 10. It is seen that the flexoelectric Pt/LFO/LNO photodetectors are very stable from 25 to 150 ℃, with a responsivity of 0.1 mA/cm^2 and detectivity of 10^8 Jones.

Table 1. Performance of the flexoelectric photodetector compared with other photo-detecting devices.

Materials	**Band gap** (eV)	**Responsivity** (A/W)	**Detectivity** (Jones)	**Response time**	**Reference**
$LaFeO_3$ film	2.7	1×10^{-4}	10^8	15 ns	This work
$BaTiO_3$ film	3.2	1.4×10^{-1}	10^{11}	15.16/16.35 s	[39]
$BaTiO_3$ ceramic	3.2	4×10^{-7}	3×10^5	0.4/1.6 s	[40]
$BaTiO_3$ ceramic	3.2	6×10^{-8}	10^5	0.5/23.0 s	[41]
$BaTiO_3$ ceramic	3.2	2×10^{-7}	4×10^5	0.5 s	[42]
$BaTiO_3$ single crystal	3.2	1×10^{-5}	1×10^8	1 ns	[43]
$Pb(Zr,Ti)O_3$ film	3.6	1.5×10^{-2}	2×10^{10}	50 ms	[44]
$(Pb,La)(Zr,Ti)O_3$ film	3.6	1.75×10^{-5}	——	——	[45]
$BiFeO_3$ film	2.67	1.5×10^{-4}	——	11.8/23.6 ns	[46]
$BiFeO_3$ ceramic	2.67	6.0×10^{-4}	10^{12}	0.6 s	[47]

In summary, we have designed and fabricated flexoelectric photodetectors by utilizing

the structural relaxation of LFO thin films grown on lattice mismatched substrates. The atomic resolution HAADF-STEM images reveal a giant strain gradient on the order of 10^6 /m in the LFO thin film, and the resulted flexoelectric polarization gives rise to a spontaneous photoresponse in the Pt/LFO/LNO/LAO devices with a responsivity of 10^{-4} A/W, detectivity of 10^8 Jones, and a response time of 15 ns. Self-powered photoresponse properties have also been reported in ferroelectric oxides, such as $BaTiO_3$ single crystals, $BiFeO_3$ ceramics, micrometer-thick $Pb(Zr,Ti)O_3$ films, and coplanar-electroded $BiFeO_3$ heterostructures, for the detection of ultraviolet light, as listed in Table 1. Our Pt/LFO/LNO/LAO photodetectors exhibit comparable or superior performance in comparison with these ferroelectric devices. More importantly, the flexoelectric photocurrents in the present work are achieved in ultrathin LFO layers of only 11 nm in thickness and our proposed concept of a flexoelectric photodetector can be applied to a wide spectrum of materials, regardless of their crystalline symmetries. These merits will facilitate the development of microminiaturized devices with diverse optoelectronic applications, such as integrated optical communication and biomedical imaging.

ASSOCIATED CONTENT

Supporting Information

Supporting information is available free of charge at website.

Materials and methods; Absorption spectra of the LFO thin films; Measuring flexoelectric coefficient by cantilever beam bending method; Electron energy loss spectra of the LFO thin films; Calculating the band structure of a LAO/LNO/LFO(~11 nm)/Pt device; Open circuit voltage with changing work function of the top electrode; Structure and strain analysis of LFO thin films on LAO and STO substrates; Photoresponse of LFO thin films; Comparison of the flexoelectric photodetector with other types of photodetectors.

AUTHOR INFORMATION

Corresponding Authors

Xiaojie Lou - Frontier Institute of Science and Technology, State Key Laboratory of Electrical Insulation and Power Equipment, and State Key Laboratory for Mechanical Behavior of Materials, Xi'an Jiaotong University, Xi'an 710049, P. R. China

Email: xlou03@mail.xjtu.edu.cn

Stephen J. Pennycook - Department of Materials Science and Engineering, National University of Singapore, 9 Engineering Drive 1, 117575, Singapore

Email: stevepennycook@gmail.com

Zheng Wen - College of Physics and Center for Marine Observation and Communications, Qingdao University, Qingdao 266071, P. R. China

Email: zwen@qdu.edu.cn

Authors

Ming Wu-Frontier Institute of Science and Technology, State Key Laboratory of Electrical Insulation and Power Equipment, and State Key Laboratory for Mechanical Behavior of Materials, Xi'an Jiaotong University, Xi'an 710049, P. R. China and Department of Materials Science and Engineering, National University of Singapore, 9 Engineering Drive 1, 117575, Singapore

Zhizheng Jiang- College of Physics and Center for Marine Observation and Communications, Qingdao University, Qingdao 266071, P. R. China

Fan Zhang- Department of Applied Physics, The Hong Kong Polytechnic University, Hung Hom, 999077 Kowloon, Hong Kong

Dongsheng Song- Ernst Ruska-Centre for Microscopy and Spectroscopy with Electrons, Forschungszentrum Jülich, D-52425 Jülich, Germany

Shoucong Ning- Department of Materials Science and Engineering, National University of Singapore, 9 Engineering Drive 1, 117575, Singapore

Mengyao Guo-Frontier Institute of Science and Technology, State Key Laboratory of Electrical Insulation and Power Equipment, and State Key Laboratory for Mechanical Behavior of Materials, Xi'an Jiaotong University, Xi'an 710049, P. R. China

Ji-yan Dai- Department of Applied Physics, The Hong Kong Polytechnic University, Hung Hom, 999077 Kowloon, Hong Kong

Author contributions

M. W. and Z. J. contributed equally in this work. Z.J fabricated the devices and characterized the photovoltaic effect under the supervision of Z.W. M.W analyzed the photovoltaic data under the supervision of Z.W and X.J.L. M.W performed the STEM characterization and analyzed the data under the supervision of S.J.P and X.J.L. F.Z conducted the measurement of flexoelectric coefficient under the supervision of J.Y.D. M.W., Z.W., X.J.L. and S.J.P. wrote the manuscript and all authors contributed to the discussion of the manuscript.

Notes

The authors declare no competing financial interest.

ACKNOWLEDGMENTS

We acknowledge the support from the National Natural Science Foundation of China (NSFC No. 51872148 and 51772238), Natural Science Foundation of Shandong

(ZR2020JQ03), the CSS project (Grant No. YK2015-0602006), the Fundamental research Funds for the Central Universities and the World-Class Universities (Disciplines) and the Characteristic Development Guidance Funds for the Central Universities. Z. W. acknowledges support from the Special Funds of the Taishan Scholar Program of Shandong Province (tsqn201812045) and the Youth Innovation Team Project of Shandong Provincial Education Department (2019KJJ012). S. J. P. thanks the National University of Singapore and the Singapore Ministry of Education under its Tier 2 grant MOE2017-T2-1-129 for support. J. Y. D. acknowledges support from the General Research Fund (GRF) of Hong Kong (Grant No. 15300018). The authors would like to thank Prof. Gustau Catalan for fruitful discussions.

REFERENCES

(1) Haeni, J.; Irvin, P.; Chang, W.; Uecker, R.; Reiche, P.; Li, Y.; Choudhury, S.; Tian, W.; Hawley, M.; Craigo, B. Room-temperature ferroelectricity in strained $SrTiO_3$. *Nature* **2004,** *430* (7001), 758.

(2) Das, S.; Tang, Y.; Hong, Z.; Gonçalves, M.; McCarter, M.; Klewe, C.; Nguyen, K.; Gómez-Ortiz, F.; Shafer, P.; Arenholz, E. Observation of room-temperature polar skyrmions. *Nature* **2019,** *568* (7752), 368.

(3) Zubko, P.; Catalan, G.; Tagantsev, A. K. Flexoelectric effect in solids. *Annu. Rev. Mater. Res.* **2013,** *43*, 387-421.

(4) Chu, B.; Zhu, W.; Li, N.; Cross, L. E. Flexure mode flexoelectric piezoelectric composites. *J. Appl. Phys.* **2009,** *106* (10), 104109.

(5) Fu, J. Y.; Zhu, W.; Li, N.; Smith, N. B.; Eric Cross, L. Gradient scaling phenomenon in microsize flexoelectric piezoelectric composites. *Appl. Phys. Lett.* **2007,** *91* (18), 182910.

(6) Zhu, W.; Fu, J. Y.; Li, N.; Cross, L. Piezoelectric composite based on the enhanced flexoelectric effects. *Appl. Phys. Lett.* **2006,** *89* (19), 192904.

(7) Zhou, W.; Chen, P.; Pan, Q.; Zhang, X.; Chu, B. Lead-free metamaterials with enormous apparent piezoelectric response. *Adv. Mater.* **2015,** *27* (41), 6349-6355.

(8) Yan, X.; Huang, W.; Kwon, S. R.; Yang, S.; Jiang, X.; Yuan, F.-G. A sensor for the direct measurement of curvature based on flexoelectricity. *Smart Mater. Struct.* **2013,** *22* (8), 085016.

(9) Qi, Y.; Kim, J.; Nguyen, T. D.; Lisko, B.; Purohit, P. K.; McAlpine, M. C. Enhanced piezoelectricity and stretchability in energy harvesting devices fabricated from buckled PZT ribbons. *Nano Lett.* **2011,** *11* (3), 1331-1336.

(10) Bhaskar, U. K.; Banerjee, N.; Abdollahi, A.; Wang, Z.; Schlom, D. G.; Rijnders, G.; Catalan, G. A flexoelectric microelectromechanical system on silicon. *Nat. Nanotechnol.* **2016,** *11* (3), 263.

(11) Shu, L.; Ke, S.; Fei, L.; Huang, W.; Catalan, G. Photoflexoelectric effect in halide perovskites. *Nat. Mater.*

2020, *19* (6).
(12) Tang, Y.; Zhu, Y.; Ma, X.; Borisevich, A. Y.; Morozovska, A. N.; Eliseev, E. A.; Wang, W.; Wang, Y.; Xu, Y.; Zhang, Z. Observation of a periodic array of flux-closure quadrants in strained ferroelectric $PbTiO_3$ films. *Science* **2015,** *348* (6234), 547-551.
(13) Lu, H.; Bark, C.-W.; De Los Ojos, D. E.; Alcala, J.; Eom, C.-B.; Catalan, G.; Gruverman, A. Mechanical writing of ferroelectric polarization. *Science* **2012,** *336* (6077), 59-61.
(14) Park, S. M.; Wang, B.; Das, S.; Chae, S. C.; Chung, J.-S.; Yoon, J.-G.; Chen, L.-Q.; Yang, S. M.; Noh, T. W. Selective control of multiple ferroelectric switching pathways using a trailing flexoelectric field. *Nat. Nanotechnol.* **2018,** *13* (5), 366.
(15) Das, S.; Wang, B.; Cao, Y.; Cho, M. R.; Shin, Y. J.; Yang, S. M.; Wang, L.; Kim, M.; Kalinin, S. V.; Chen, L.-Q. Controlled manipulation of oxygen vacancies using nanoscale flexoelectricity. *Nat. Commun.* **2017,** *8* (1), 615.
(16) Das, S.; Wang, B.; Paudel, T. R.; Park, S. M.; Tsymbal, E. Y.; Chen, L.-Q.; Lee, D.; Noh, T. W. Enhanced flexoelectricity at reduced dimensions revealed by mechanically tunable quantum tunnelling. *Nat. Commun.* **2019,** *10* (1), 537.
(17) Wang, W.; Chen, X.; Sun, Q.; Xin, T.; Ye, M. Tailoring the negative electrocaloric effect of $PbZrO_3$ antiferroelectric thin films by Yb doping. *J. Alloy. Compd.* **2020,** *830*, 154581.
(18) Yang, M.-M.; Kim, D. J.; Alexe, M. Flexo-photovoltaic effect. *Science* **2018,** *360* (6391), 904-907.
(19) Lee, D.; Yang, S. M.; Yoon, J. G.; Noh, T. W. Flexoelectric rectification of charge transport in strain-graded dielectrics. *Nano Lett.* **2012,** *12* (12), 6436-6440.
(20) Zhang, F.; Lv, P.; Zhang, Y.; Huang, S.; Wong, C.-M.; Yau, H.-M.; Chen, X.; Wen, Z.; Jiang, X.; Zeng, C. Modulating the Electrical Transport in the Two-Dimensional Electron Gas at $LaAlO_3/SrTiO_3$ Heterostructures by Interfacial Flexoelectricity. *Phys. Rev. Lett.* **2019,** *122* (25), 257601.
(21) Lee, D.; Yoon, A.; Jang, S.; Yoon, J.-G.; Chung, J.-S.; Kim, M.; Scott, J.; Noh, T. Giant flexoelectric effect in ferroelectric epitaxial thin films. *Phys. Rev. Lett.* **2011,** *107* (5), 057602.
(22) Chu, K.; Jang, B.-K.; Sung, J. H.; Shin, Y. A.; Lee, E.-S.; Song, K.; Lee, J. H.; Woo, C.-S.; Kim, S. J.; Choi, S.-Y. Enhancement of the anisotropic photocurrent in ferroelectric oxides by strain gradients. *Nat. Nanotechnol.* **2015,** *10* (11), 972.
(23) Maranganti, R.; Sharma, P. Atomistic determination of flexoelectric properties of crystalline dielectrics. *Phys. Rev. B* **2009,** *80* (5), 054109.
(24) Liu, X.; Zhang, F.; Long, P.; Lu, T.; Zeng, H.; Liu, Y.; Withers, R. L.; Li, Y.; Yi, Z. Anomalous Photovoltaic Effect in Centrosymmetric Ferroelastic $BiVO_4$. *Adv. Mater.* **2018,** *30* (44), 1801619.
(25) Tang, Y.; Zhu, Y.; Ma, X. On the benefit of aberration-corrected HAADF-STEM for strain determination and its application to tailoring ferroelectric domain patterns. *Ultramicroscopy* **2016,** *160*, 57-63.
(26) Gao, P.; Yang, S.; Ishikawa, R.; Li, N.; Feng, B.; Kumamoto, A.; Shibata, N.; Yu, P.; Ikuhara, Y. Atomic-scale measurement of flexoelectric polarization at $SrTiO_3$ dislocations. *Phys. Rev. Lett.* **2018,** *120* (26), 267601.
(27) Hÿtch, M. J.; Putaux, J.-L.; Pénisson, J.-M. Measurement of the displacement field of dislocations to 0.03 Å by electron microscopy. *Nature* **2003,** *423* (6937), 270-273.
(28) Hÿtch, M. J.; Snoeck, E.; Kilaas, R. Quantitative measurement of displacement and strain fields from HREM micrographs. *Ultramicroscopy* **1998,** *74* (3), 131-146.
(29) Biancoli, A.; Fancher, C. M.; Jones, J. L.; Damjanovic, D. Breaking of macroscopic centric symmetry in paraelectric phases of ferroelectric materials and implications for flexoelectricity. *Nat. Mater.* **2015,** *14* (2), 224-229.
(30) Abdollahi, A.; Vásquez-Sancho, F.; Catalan, G. Piezoelectric mimicry of flexoelectricity. *Phys. Rev. Lett.* **2018,** *121* (20), 205502.

(31) Tan, H.; Verbeeck, J.; Abakumov, A.; Van Tendeloo, G. Oxidation state and chemical shift investigation in transition metal oxides by EELS. *Ultramicroscopy* **2012,** *116*, 24-33.
(32) Biškup, N.; Salafranca, J.; Mehta, V.; Oxley, M. P.; Suzuki, Y.; Pennycook, S. J.; Pantelides, S. T.; Varela, M. Insulating ferromagnetic $LaCoO_{3-\delta}$ films: a phase induced by ordering of oxygen vacancies. *Phys. Rev. Lett.* **2014,** *112* (8), 087202.
(33) Kim, Y.-M.; He, J.; Biegalski, M. D.; Ambaye, H.; Lauter, V.; Christen, H. M.; Pantelides, S. T.; Pennycook, S. J.; Kalinin, S. V.; Borisevich, A. Y. Probing oxygen vacancy concentration and homogeneity in solid-oxide fuel-cell cathode materials on the subunit-cell level. *Nat. Mater.* **2012,** *11* (10), 888-894.
(34) Pennycook, S.; Zhou, H.; Chisholm, M.; Borisevich, A.; Varela, M.; Gazquez, J.; Pennycook, T.; Narayan, J. Misfit accommodation in oxide thin film heterostructures. *Acta Mater.* **2013,** *61* (8), 2725-2733.
(35) Chu, K.; Jang, B.-K.; Sung, J. H.; Shin, Y. A.; Lee, E.-S.; Song, K.; Lee, J. H.; Woo, C.-S.; Kim, S. J.; Choi, S.-Y. Enhancement of the anisotropic photocurrent in ferroelectric oxides by strain gradients. *Nat. Nanotechnol.* **2015,** *10* (11), 972-979.
(36) Yang, S.; Seidel, J.; Byrnes, S.; Shafer, P.; Yang, C.-H.; Rossell, M.; Yu, P.; Chu, Y.-H.; Scott, J.; Ager, J. Above-bandgap voltages from ferroelectric photovoltaic devices. *Nat. Nanotechnol.* **2010,** *5* (2), 143-147.
(37) Sheu, Y. M.; Trugman, S. A.; Park, Y.-S.; Lee, S.; Yi, H. T.; Cheong, S.-W.; Jia, Q. X.; Taylor, A. J.; Prasankumar, R. P. Ultrafast carrier dynamics and radiative recombination in multiferroic $BiFeO_3$. *Appl. Phys. Lett. 100* (24), 242904.
(38) Koppens, F.; Mueller, T.; Avouris, P.; Ferrari, A.; Vitiello, M.; Polini, M. Photodetectors based on graphene, other two-dimensional materials and hybrid systems. *Nat. Nanotechnol.* **2014,** *9* (10), 780.
(39) Pandey, B.; Dias, S.; Nanda, K.; Krupanidhi, S. Deep UV-Vis photodetector based on ferroelectric/semiconductor heterojunction. *J. Appl. Phys.* **2017,** *122* (23), 234502.
(40) Tang, Y.; Zhu, Y.; Liu, Y.; Wang, Y.; Ma, X. Giant linear strain gradient with extremely low elastic energy in a perovskite nanostructure array. *Nat. Commun.* **2017,** *8*, 15994.
(41) Ma, N.; Yang, Y. Enhanced self-powered UV photoresponse of ferroelectric $BaTiO_3$ materials by pyroelectric effect. *Nano Energy* **2017,** *40*, 352-359.
(42) Ma, N.; Yang, Y. Boosted photocurrent in ferroelectric $BaTiO_3$ materials via two dimensional planar-structured contact configurations. *Nano Energy* **2018,** *50*, 417-424.
(43) Li, J. K.; Ge, C.; Jin, K.-j.; Du, J.-y.; Yang, J.-t.; Lu, H.-b.; Yang, G.-z. Self-driven visible-blind photodetector based on ferroelectric perovskite oxides. *Appl. Phys. Lett. 110* (14), 142901.
(44) Dou, L.; Yang, Y. M.; You, J.; Hong, Z.; Chang, W.-H.; Li, G.; Yang, Y. Solution-processed hybrid perovskite photodetectors with high detectivity. *Nat. Commun.* **2014,** *5*, 5404.
(45) Gan, B. K.; Yao, K.; Lai, S. C.; Goh, P. C.; Chen, Y. F. A Ferroelectric Ultraviolet Detector With Constructive Photovoltaic Outputs. *IEEE Electr. Device L. 32* (5), 5750019-149.
(46) Xing, J.; Guo, E.-J.; Dong, J.; Hao, H.; Zheng, Z.; Zhao, C. High-sensitive switchable photodetector based on $BiFeO_3$ film with in-plane polarization. *Appl. Phys. Lett.* **2015,** *106* (3), 033504.
(47) Qi, J.; Ma, N.; Ma, X.; Adelung, R.; Yang, Y. Enhanced photocurrent in $BiFeO_3$ materials by coupling temperature and thermo-phototronic effects for self-powered ultraviolet photodetector system. *ACS Appl. Mater. Inter.* **2018,** *10* (16), 13712-13719.

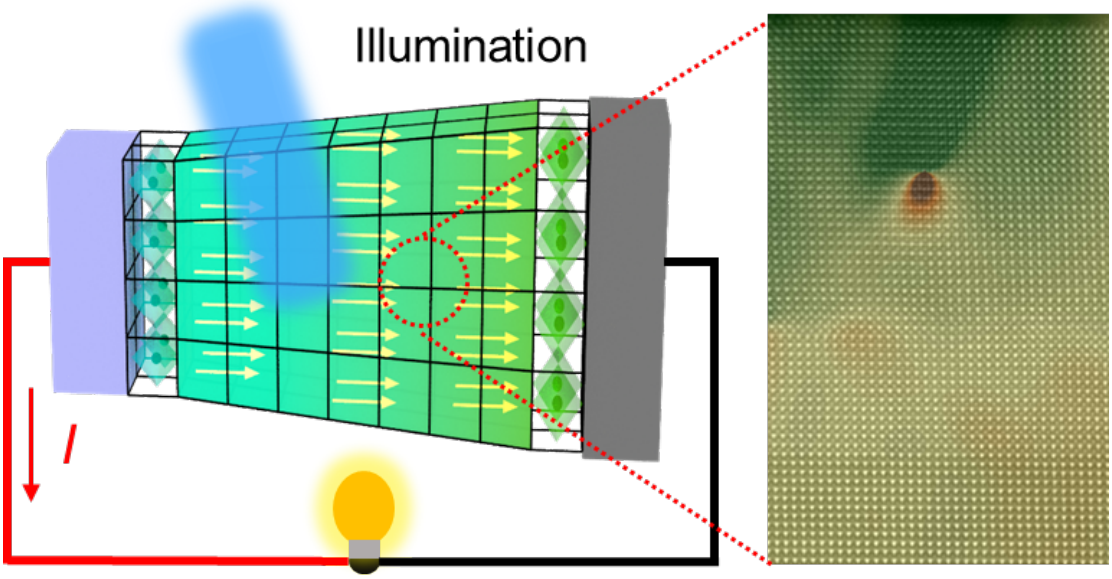

TOC Graphic

Figure Captions

Figure 1. Flexoelectric effect caused by strain gradients of different scales. Flexoelectric polarization induced by (a) asymmetric application of stress in a trapezoid structure, (b) bending a microribbon and (c) the relaxation of mismatch strain in a thin-film heterostructure. The yellow arrows indicate the flexoelectric polarization. In the strained-engineered heterostructure, photoexcited carriers can be separated by the flexoelectric polarization and thus generate a photocurrent. (d) Schematic of the energy bands in the partially relaxed heterostructure with flexoelectric polarization. (e) The solar spectrum and corresponding band gaps of the materials with reported flexoelectric effects.

Figure 2. Misfit strain relaxation of LFO thin films on LAO and STO substrates. Schematics of strain relaxation and lattice distortion of (a) LFO/LNO/LAO and (b) LFO/LNO/STO, respectively. HAADF images of (c) LFO/LNO/LAO and (e) LFO/LNO/STO, respectively. In (c), the red dashed cycle indicates a dislocation. The in-plane strain e_{xx} of (d) LFO/LNO/LAO and (f) LFO/LNO/STO calculated from the HAADF images (c and e) by the GPA method. In-plane strain e_{xx} and the corresponding strain gradient $\partial e_{xx}/\partial z_k$ of the (g) LFO/LNO/LAO and (h) LFO/LNO/STO heterostructures along the blue thick arrows in (d) and (f), respectively. (i) EELS spectra of the Fe L edge in different regions of the LFO/LNO/LAO (profile lines 1, 2) and LFO/LNO/STO (profile lines 3, 4), respectively.

Figure 3. The mechanisms of photovoltaic effects in Pt/LFO/LNO/LAO devices. (a) Band diagram of the Pt/LFO/LNO heterostructure when only considering Schottky contact. The Schottky barrier $\emptyset'_{B01}$ and $\emptyset'_{B02}$ at Pt/LFO and LFO/LNO interfaces are 1.6 eV and 0.8 eV, respectively. (b) Band diagram of the Pt/LFO/LNO heterostructure when considering Schottky contact and the existence of flexoelectric polarization. The Schottky barrier $\emptyset_{\mathrm{B01}}$ and $\emptyset_{\mathrm{B02}}$ at Pt/LFO and LFO/LNO interfaces are 1.22 eV and 1.25 eV, respectively. The blue and yellow balls represent photogenerated electrons and holes and the arrows denote their flow direction. The (c) The photovoltaic effects dominated by the flexoelectric polarization (green solid line) and the interfacial Schottky barrier (red dashed line) in the Pt/LFO/LNO devices.

Figure 4. The flexoelectric photovoltaic effects in Pt/LFO/LNO devices. (a) *J-V* curves of the ~11 nm-thick Pt/LFO/LNO on LAO and STO substrates with and without illumination. The inset shows the J_{sc} and V_{oc} of Pt/LFO/LNO/LAO as a function of LFO thickness. (b) Illumination *J-V* curves of a 35 nm Pt/LFO/LNO/LAO device with increasing power density of blue light. The inset shows the power-density-dependent J_{sc}. (c) Time-dependent J_{sc} of the 35 nm Pt/LFO/LNO/LAO as the light is switched on and off. The inset shows the nanosecond response of the device under illumination of a nanosecond pulse laser. (d) Responsivity and detectivity of the 35 nm Pt/LFO/LNO/LAO over a wide temperature range from 25 to 150 ℃.